

## Universal evaporation dynamics of a confined sessile droplet

Lalit Bansal, Sandeep Hatte, Saptarshi Basu, and Suman Chakraborty

Citation: *Appl. Phys. Lett.* **111**, 101601 (2017); doi: 10.1063/1.4996986

View online: <http://dx.doi.org/10.1063/1.4996986>

View Table of Contents: <http://aip.scitation.org/toc/apl/111/10>

Published by the [American Institute of Physics](#)

---

### Articles you may be interested in

[Lattice Boltzmann simulations for water coalescence](#)

*Applied Physics Letters* **111**, 101602 (2017); 10.1063/1.4985264

[Droplet evaporation with complexity of evaporation modes](#)

*Applied Physics Letters* **110**, 031602 (2017); 10.1063/1.4974292

[Molecular beam epitaxial growth and characterization of AlN nanowall deep UV light emitting diodes](#)

*Applied Physics Letters* **111**, 101103 (2017); 10.1063/1.4989551

[Single orbital angular mode emission from externally feed-backed vertical cavity surface emitting laser](#)

*Applied Physics Letters* **111**, 101102 (2017); 10.1063/1.4989479

[3D tomography of cells in micro-channels](#)

*Applied Physics Letters* **111**, 103701 (2017); 10.1063/1.4986392

[High performance terahertz metasurface quantum-cascade VECSEL with an intra-cryostat cavity](#)

*Applied Physics Letters* **111**, 101101 (2017); 10.1063/1.4993600

---



**HIGH-VOLTAGE AMPLIFIERS AND  
ELECTROSTATIC VOLTMETERS**

ENABLING RESEARCH AND  
INNOVATION IN DIELECTRICS,  
MICROFLUIDICS,  
MATERIALS, PLASMAS AND PIEZOS

## Universal evaporation dynamics of a confined sessile droplet

Lalit Bansal,<sup>1</sup> Sandeep Hatte,<sup>1</sup> Saptarshi Basu,<sup>1,a)</sup> and Suman Chakraborty<sup>2,a)</sup>

<sup>1</sup>Department of Mechanical Engineering, Indian Institute of Science, Bangalore 560012, India

<sup>2</sup>Department of Mechanical Engineering, Indian Institute of Technology Kharagpur, Kharagpur 721302, India

(Received 20 July 2017; accepted 24 August 2017; published online 5 September 2017)

Droplet evaporation under confinement is ubiquitous to multitude of applications such as microfluidics, surface patterning, and ink-jet printing. However, the rich physics governing the universality in the underlying dynamics remains grossly elusive. Here, we bring out hitherto unexplored universal features of the evaporation dynamics of a sessile droplet entrapped in a 3D confined fluidic environment. We show, through extensive set of experiments and theoretical formulations, that the evaporation timescale for such a droplet can be represented by a unique function of the initial conditions. Moreover, using same theoretical considerations, we are able to trace and universally merge the volume evolution history of the droplets along with evaporation lifetimes, irrespective of the extent of confinement. We also showcase the internal flow transitions caused by spatio-temporal variation of evaporation flux due to confinement. These findings may be of profound importance in designing functionalized droplet evaporation devices for emerging engineering and biomedical applications. *Published by AIP Publishing.* [<http://dx.doi.org/10.1063/1.4996986>]

In depth understanding and subsequent control of droplet evaporation has been a topic of active research due to its fundamental scientific importance in dictating the pertinent wetting characteristics as well as its implications in diverse applications ranging from spray drying,<sup>1–3</sup> surface patterning,<sup>4–6</sup> to DNA analysis.<sup>7,8</sup>

Evaporation rate in sessile droplets is dependent on various factors such as substrate characteristics, vapor diffusivity, and ambient conditions. For instance, evaporation may be dramatically affected by varying the vapor concentration in the vicinity of the evaporating droplet. For example, it was shown<sup>9</sup> that two water-PG (Propylene Glycol) droplets can attract each other (long range interactions) due to increased vapor concentration between them. Furthermore, local increase in vapor concentration may increase the evaporation lifetime and induce asymmetric internal flow.<sup>10–13</sup> In addition, any evaporating sessile droplet exhibits distinctive modes of evaporation (constant contact radius: CCR, constant contact angle: constant contact angle (CCA), Mixed) altering the consequent vapor field as well as internal flow characteristics in a rather non-trivial manner. This, in turn, may modulate self-assembly of particles leading to alteration in the morphology of the final precipitate.<sup>10–13</sup> This can have significant practical implications in emerging applications such as 3D printing and surface coating.

Understanding such evaporation dynamics in confined fluidic environment is crucial in the fields of microfluidics<sup>14,15</sup> and energy conversion devices like Proton Exchange Membrane fuel cell.<sup>16</sup> For instance, in microfluidics, evaporation based micropumps may be used for sample transportation in lab on chip devices.

Here, we bring out distinctive universal features of evaporation dynamics of a sessile droplet in a confined 3D fluidic environment. In effect, we subject water droplets to different vapor concentration fields by entrapping them in

mini-channels of various confinements. While 1D channels were somewhat studied,<sup>17</sup> 3D effects remain largely unexplored. Vapor flux from confined droplets is entrapped in a small space accompanied by dynamical alterations in the underlying evaporation characteristics. Our experimental results and theoretical calculations demonstrate that the droplet evaporation timescale can be universally merged to a unique normalized function of the initial conditions, which include the effects of the channel dimensions (length, width, and height) and initial droplet volume. In addition, we are also able to show that the regression history of the contact radius and the contact angle for each evaporation mode can also be represented by universal functional profiles.

A  $1.5 \pm 0.1 \mu\text{l}$  DI water droplet is deployed at the geometric center of a PDMS channel (see [supplementary material](#)). Droplet is confined by the channel walls along width (W) and height (H), but is open to ambient along channel length (L) [Fig. 1(a)]. Experiments are swept across a total of 50 different combinations of channel configurations (hereafter channel dimensions are to be read in the form  $W \times H \times L$ ; unless otherwise specified) (Table S1, [supplementary material](#)). During the entire period of evaporation, ambient conditions (outside the channel) are maintained at  $25 \pm 2^\circ\text{C}$  and  $45 \pm 3\%$  relative humidity. Temporal changes in the droplet shape are captured by Nikon D7200 SLR camera at 1 fps. For flow visualization, side and front view images are captured at 1 fps and overlapped to obtain the flow streaklines inside the evaporating droplet. On the other hand, for quantification of flow velocity, a total of 100 bottom view images [micro-particle image velocimetry ( $\mu\text{PIV}$ )] are acquired in a plane at a height of  $\frac{h}{h_0} \approx 0.6$  from droplet base ( $h_0$ : instantaneous droplet height). The images are acquired during the initial ( $\frac{t}{t_e} \approx 0.1$ ) and final stages ( $\frac{t}{t_e} \approx 0.8$ ) of evaporation ( $t_e$ : droplet lifetime) and processed using cross correlation algorithm (see [supplementary material](#) for details).

For an unconfined droplet evaporating on a hydrophobic substrate, the diffusion of water vapor from liquid-air interface to the ambient is the rate determining step. On the other

<sup>a)</sup>Authors to whom correspondence should be addressed: sbasu@mecheng.iisc.ernet.in and suman@mech.iitkgp.ernet.in

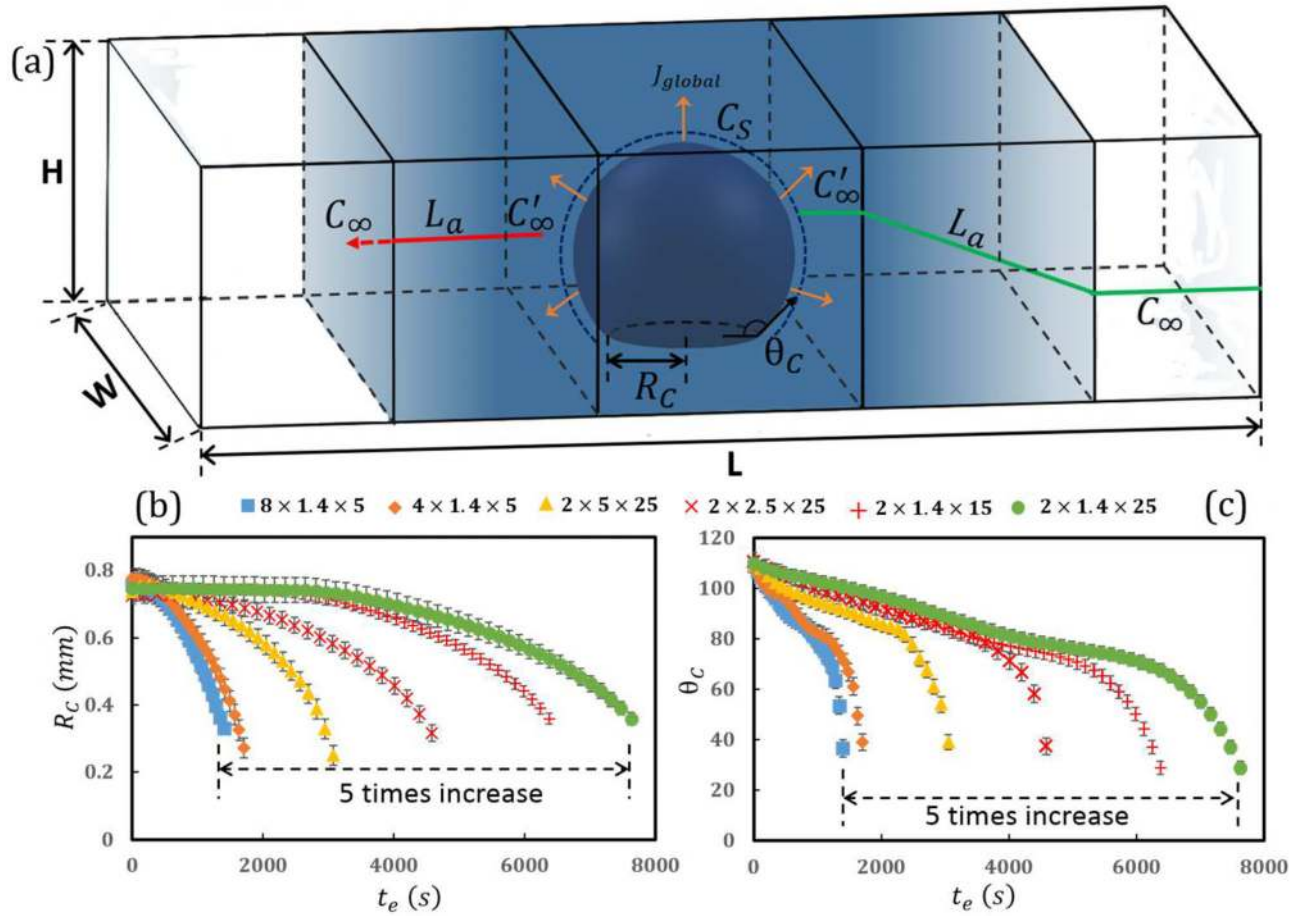


FIG. 1. (a) Schematic of evaporation model of a sessile droplet inside a PDMS channel confined along width ( $W$ ) and height ( $H$ ), and open to ambient along length ( $L$ ). Water vapor concentration in the confined region increases to  $c'_\infty$  and approaches to ambient vapor concentration ( $c_\infty$ ) along channel length over a distance  $L_a (< L/2)$  termed as accumulation length. Temporal variation of (b) contact radius and (c) contact angle across different combinations of channel dimensions ( $W \times H \times L$ ).

hand, for a confined droplet, a wedge region is formed between the channel wall, base, and droplet periphery (Fig. S3, [supplementary material](#)). Thus, mobility of the vapour leaving the droplet-air interface is reduced as a direct effect of close channel walls and the wedge, which leads to entrapment of the vapors of relatively higher concentration,  $c'_\infty$  ( $> c_\infty$ ) inside the channel thereby prolonging the droplet lifetime (see Fig. S4 in [supplementary material](#) for temporal variation in  $c'_\infty$ ). It is to be noted that  $c'_\infty$  is averaged around the droplet in polar and azimuthal directions. Evaporation results in the vapors filling up the confined cross section and subsequently propagation along the channel length. Entrapped enhanced vapor concentration field ( $c'_\infty$ ) linearly relaxes to the ambient concentration ( $c_\infty$ ) over  $L_a$  [accumulation length in Fig. 1(a)].  $L_a$  shows negligible temporal variation over majority of the droplet lifetime. From Figs. 1(b) and 1(c), about 5 times increase in droplet lifetime is observed across the extreme limits of channel configurations (from least confined ( $8 \times 1.4 \times 5$ ) to most confined ( $2 \times 1.4 \times 25$ )). Increment in channel width and/or height increases the cross-sectional area facilitating relaxation of the trapped vapor field concentration. This in turn results in reduction of droplet lifetime. Contrarily, droplet lifetime increases on increasing the channel length.<sup>17</sup> It is observed that there is a 40%–60% decrease in droplet lifetime as the channel width is increased from 2 mm to 8 mm (keeping height constant) or when the

height is increased from 1.4 mm to 5 mm (keeping width constant). However, it is to be noted that the evaporation modes remain unchanged regardless of confinement with timescales given as:  $0.4 \times t_e$  for CCR (i.e., 40% of the droplet lifetime is spent in CCR mode),  $0.3 \times t_e$  for CCA, and  $0.3 \times t_e$  for mixed.

In order to obtain the theoretical timescales of droplet evaporation inside a channel, it is important to understand the evaporation dynamics of a confined droplet. A confined droplet evaporation is a two-step process. First, there is diffusion of water vapor from interface ( $c_s$ —saturated vapor concentration) to the region of vapor entrapment ( $c'_\infty$ ), which is followed by diffusion from  $c'_\infty$  to the ambient ( $c_\infty$ ) [Fig. 1(a)]. Thus, for a confined droplet, diffusion from droplet vicinity to ambient is the rate determining step.  $c'_\infty$  (and  $L_a$ ) shows negligible temporal fluctuations except in the final stage (Fig. S4 in [supplementary material](#)). The instantaneous spatially averaged rate of evaporation from interface to the region of vapor entrapment is given by

$$\frac{dV}{dt} = \frac{-J_{avg} A_s}{\rho} = \frac{-2\pi D M R_c f(\theta) (c_s - \overline{c'_\infty})}{\rho}, \quad (1)$$

where  $V$  is the instantaneous droplet volume,  $J_{avg}$  is spatially averaged evaporation flux,  $A_s$  is the surface area of the droplet,  $D$  is the diffusion coefficient,  $M$  is molecular mass,  $R_c$  is the instantaneous contact radius of the droplet,  $\rho$  is the

density of the working fluid,  $\overline{c'_\infty} \sim c'_\infty$  (Fig. S4, [supplementary material](#)) is the time averaged enhanced vapor concentration around the droplet, and  $f(\theta)$  is a function of the instantaneous contact angle ( $\theta$ ) of spherical cap shaped sessile droplets. Its empirical polynomial form ( $f(\theta) = (0.00008957 + 0.633\theta + 0.116\theta^2 - 0.08878\theta^3 + 0.01033\theta^4) / \sin\theta$ , for  $\theta > 10^\circ$ ) was given in Refs. 18–21. It is to be noted that although there are local variations in the evaporation flux ( $J_{local}$ ) around the droplet in both polar and azimuthal directions, average evaporation flux [ $J_{avg}$ ; Fig. 1(a)] has been considered in Eq. (1). As can be seen from Fig. S1 of [supplementary material](#), the droplet volume decays non-linearly with time as the evaporation progresses. This non-linearity is mainly because of the inherent slip of three phase contact line (in CCA and mixed mode). However, the extent of non-linearity can be quantified using the average rate of change of droplet volume in terms of initial rate as  $|\frac{dV}{dt}|_{avg} = A|\frac{dV}{dt}|_{t=0}$ , where A is a constant (Fig. 2), with a value  $\sim 0.72$ . This value agrees well with the data obtained from literature.<sup>21,22</sup>

Hence, the average rate of droplet volume regression can be written as

$$\frac{dV}{dt}_{avg} = A \frac{-2\pi DMR_{ci}f(\theta_i)(c_s - \overline{c'_\infty})}{\rho}, \quad (2)$$

where  $R_{ci}$  is the initial contact radius and  $\theta_i$  is the initial contact angle. Approximating  $|\frac{dV}{dt}_{avg}|$  by  $\frac{V_d}{t_{e,c}}$  ( $V_d$ : initial droplet volume and  $t_{e,c}$ : lifetime of a confined droplet) in Eq. (2), we get

$$\frac{V_d}{t_{e,c}} = \frac{A \cdot 2\pi DMR_{ci}f(\theta_i)(c_s - \overline{c'_\infty})}{\rho}. \quad (3)$$

On the other hand, average rate of evaporation from channel to ambient is

$$\frac{dV}{dt}_{avg} = \frac{-DM(WH)(\overline{c'_\infty} - c_\infty)}{\rho \overline{L}_a}, \quad (4)$$

where  $\overline{L}_a \left[ = \frac{WH(\overline{c'_\infty} - c_\infty)}{2\pi R_{ci}f(\theta_i)(c_s - \overline{c'_\infty})} \right]$  by comparing Eqs. (2) and (4) is the temporally averaged accumulation length over the

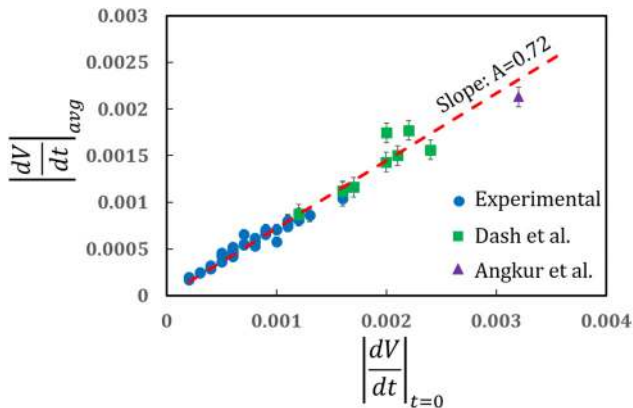


FIG. 2. Linear relationship between the average and initial rate of droplet volume reduction. The linearity agrees with the experimental data from Refs. 21 and 22.

droplet lifetime.  $\overline{L}_a$  is a linear function of channel length ( $L$ ) (Fig. S2 of [supplementary material](#) and also Ref. 17) for all configurations. Thus,  $\overline{L}_a = kL$  with  $k \approx 0.16$ . Equating (2) and (4), we have

$$(c_s - \overline{c'_\infty}) = \frac{WH(c_s - c_\infty)}{(A2\pi R_{ci}f(\theta_i)kL + WH)}. \quad (5)$$

Substituting Eq. (5) in (3), and rearranging we get

$$t_{e,c} = \frac{V_d k L}{\alpha(WH)} + \frac{V_d}{\alpha(2\pi R_{ci}f(\theta_i))}, \quad (6)$$

where  $\alpha = \frac{DM(c_s - c_\infty)}{\rho}$ . In Eq. (6), the second term on the right hand side corresponds to the lifetime of an unconfined droplet ( $t_{e,u} = \frac{V_d}{\alpha(2\pi R_{ci}f(\theta_i))}$ ). Thus, using this equation along with the initial experimental ( $R_{ci}, \theta_i$ ) conditions, theoretical timescale for complete drying of unconfined droplet can be estimated. Additionally, the first term in Eq. (6) represents the contribution of confinement. Thus, Eq. (6) can be rewritten as

$$\frac{t_{e,c}}{t_{e,u}} = (2\pi f(\theta_i)Ak) \left( \frac{LR_{ci}}{WH} \right) + 1. \quad (7)$$

Equation (7) (also Fig. 3) dictates that the normalized evaporation timescale when plotted against  $\frac{LR_{ci}}{WH}$  (extent of confinement) should exhibit a linear trend with a slope  $(2\pi f(\theta_i)Ak)$ . The experimental values of  $\frac{t_{e,c}}{t_{e,u}}$  are found to be in excellent agreement with the prediction of Eq. (7). We propose that if the lifetime of an unconfined droplet is known *a priori*, Eq. (7) can be used to predict the lifetime of the same droplet in any confined channel. To study the effect of initial droplet volume, experiments are repeated for a lower volume of  $1 \mu\text{l}$  for which there is decrease in  $R_{ci}$  (from  $\sim 0.75 \text{ mm}$  to  $\sim 0.65 \text{ mm}$ ) while  $\theta_i$  remains same. Even for a lower volume, the experimental lifetime data are in good agreement with the theoretical prediction [Eq. (7)] that is intrinsically valid for  $\theta > 90^\circ$ . Figure 3 shows that as  $W, H \rightarrow \infty$ , and/or  $L \rightarrow 0$ , the lifetime of confined cases approach to that of an unconfined case (i.e.,  $\frac{t_{e,c}}{t_{e,u}} \rightarrow 1$ ). Moreover, when the experimental timescales for different confinement levels are normalized by the corresponding theoretical values, the regression history for droplet contact radius and contact angle are found to undergo universal merger (within an error

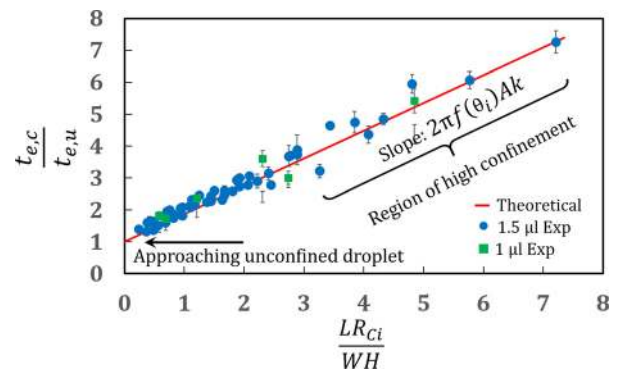


FIG. 3. Universal representation of confined droplet lifetime (normalized by lifetime of unconfined droplet) with the extent of channel confinement for  $V_1 (= 1.5 \mu\text{l})$  and  $V_2 (= 1 \mu\text{l})$ .

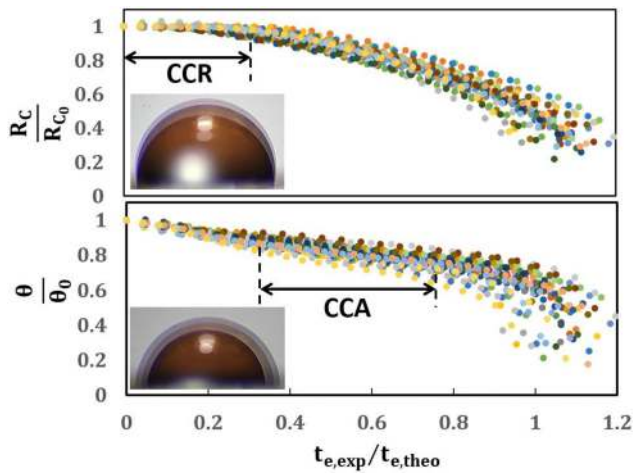


FIG. 4. Merger of temporal variations in contact radius and contact angle data across all combinations of channel configurations ( $W \times H \times L$ ) when normalized by  $t_{e,theo}$ .

of 2%–3% standard deviation) (Fig. 4). However, there is some deviation (8%–10% standard deviation) in mixed mode regime.

In the previous paragraph, we delved into the global aspects of evaporation dynamics using the spatially averaged evaporation flux ( $J_{avg}$ ). For a confined droplet, evaporation flux =  $f(\theta, \varphi, t)$ , where  $\theta$  is the polar direction and  $\varphi$  the azimuthal direction. Three key evaporation fluxes around a confined droplet are  $J_{open}$ ,  $J_{top}$ , and  $J_{wall}$ : evaporation flux towards the open, top section, and wall side of the channel, respectively. Spatial variations in evaporation flux can be represented by  $dJ$ . However, it is difficult to calculate  $J$  analytically for confined droplets. For a confined droplet, evaporation is mostly suppressed on the sides closer to the wall due to entrapment of vapors in the wedge region (Fig. S3, [supplementary material](#)) as explained earlier. Vapor from the droplet can escape only from two sides facing the exit of the channel, thus resulting in  $J_{open} > J_{wall}, J_{top}$ . Thus, the maximum spatial variation in evaporation flux in the azimuthal and polar directions can be represented as  $\Delta J_a = J_{open} - J_{wall}$  and  $\Delta J_p = J_{open} - J_{top}$ , respectively. This spatio-temporal variation in evaporation flux modifies the flow profile from radially outward (unconfined droplet<sup>10</sup>) to directional (confined

droplet) (Fig. 5; top view)<sup>17</sup> inducing a local velocity,  $v_l \propto dJ$ , and maximum velocity,  $|v_{max}| \propto \Delta J_{max} (\Delta J_a \text{ or } \Delta J_p)$ . On the open side, buoyancy driven re-circulatory flow is created inside the droplet with central streamlines moving up towards the apex region. However, for high confinements ( $W$ : 2 to 4 mm), since evaporation is maximum on the exposed portion of the droplet, the flow follows a curved path along the open side in the equatorial plane [Figs. 5(a) and 5(c); side view and multimedia view corresponding to Fig. 5 and [supplementary material](#)]. Furthermore, evaporation suppression near the walls results in a directional flow from wall to open side of the channel (seen in the bottom view).

However, as the evaporation continues, the wedge effect (Fig. S3, [supplementary material](#)) relaxes ( $J_{wall}$  increases), leading to restoration of the flow field to its unconfined counterpart (Fig. S5, [supplementary material](#)). Quantitatively, as a result of increased local vapor concentration inside the channel (decrease in  $\Delta J_{max}$ ), there is a decrease in velocity for confined droplet ( $\frac{|v_{max,c}|}{|v_{max,u}|} \approx 0.24$  for confinement of 2 mm  $\times$  1.4 mm  $\times$  5 mm). Wall effect is also reduced with the increase in channel width. Thus, as shown in Fig. 5(c), for 8 mm width channel, the internal flow is similar to unconfined droplet for the entire lifetime. Increasing the channel width also decreases the vapor concentration, thereby leading to enhanced evaporation. This, in turn, triggers augmented velocity (for instance, 1.5  $\mu\text{m/s}$  for 2 mm width to 4  $\mu\text{m/s}$  for 8 mm width channel). However, the velocity magnitude is lower as compared to unconfined scenario since vapor diffusion is still restricted by the upper wall. It is to be noted that for channels with greater heights, even though there is an increase in velocity (similar to higher width), the flow profile remains similar to the most confined scenario since there is no relaxation in the wedge effect.

To summarize, we have formulated a generalized theoretical framework for quantifying the effects of 3D confinements on droplet evaporation, supported by experimental data. We have reported four major findings. First, conventional diffusion equation can be modified to theoretically predict the timescales of any evaporating droplet on a hydrophobic substrate using the initial contact radius, contact angle, and ambient conditions. Second, lifetime of a confined

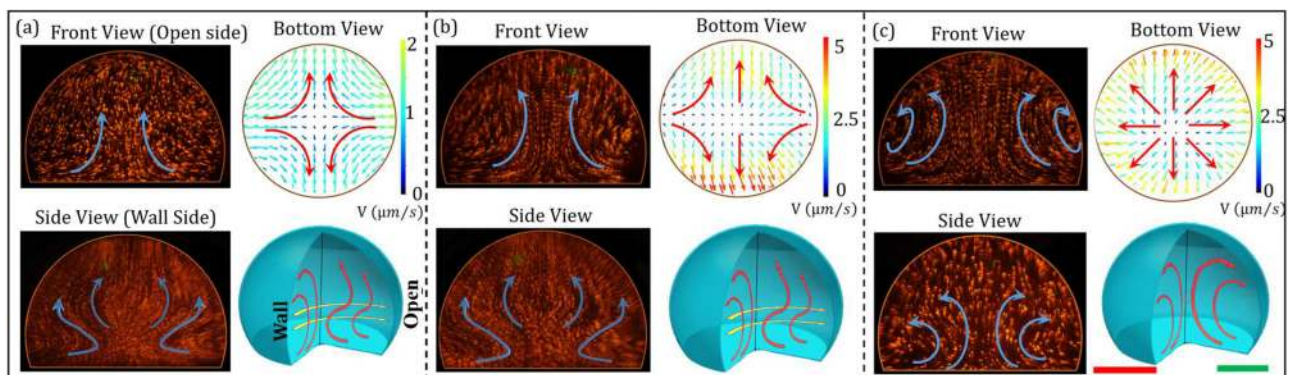


FIG. 5. Internal flow visualization (front view and side view), flow field vectors (top view) and pictorial flow representation at the initial stage ( $\frac{t}{t_e} \approx 0.1$ ) of droplet evaporation (a) confined along width and height (2  $\times$  1.4  $\times$  5) (b) confined along width and relaxed along height (2  $\times$  5  $\times$  5) (c) relaxed along width and confined along height (8  $\times$  1.4  $\times$  5). Scale bar for front view and side view flow (represented in red), and for top view vector field (represented in green) equals to 500  $\mu\text{m}$  each. Flow field vectors from the top view are investigated in a plane at a height of  $\frac{h}{h_0} \approx 0.6$  from the droplet three phase contact line, where  $h_0$  is the instantaneous droplet height. [Multimedia view for Figs. 5(a) and 5(b); side view] [URL: <http://dx.doi.org/10.1063/1.4996986.1>]

droplet is related to the corresponding unconfined droplet by a universal function, irrespective of confinement. Third, we have shown that irrespective of confinement, regression history of individual evaporation modes can also be merged using a universal description. Finally, the presence of channel walls upsets the uniformity of local evaporation flux leading to complicated internal flow transitions. These findings may turn out to be of profound importance in diverse applications ranging from surface patterning to microfluidics.

See [supplementary material](#) for extended experimental methodology and additional experimental data for theoretical analysis and flow field visualization.

- <sup>1</sup>A. Carné-Sánchez, I. Imaz, M. Cano-Sarabia, and D. Maspoch, "A spray-drying strategy for synthesis of nanoscale metal–organic frameworks and their assembly into hollow superstructures," *Nat. Chem.* **5**(3), 203 (2013).
- <sup>2</sup>N. Tsapis, D. Bennett, B. Jackson, D. A. Weitz, and D. A. Edwards, "Trojan particles: Large porous carriers of nanoparticles for drug delivery," *Proc. Natl. Acad. Sci. U.S.A.* **99**(19), 12001 (2002).
- <sup>3</sup>C. Edwards, A. Arbabi, B. Bhaduri, X. Wang, R. Ganti, P. J. Yunker, A. G. Yodh, G. Popescu, and L. Goddard, "Measuring the nonuniform evaporation dynamics of sprayed sessile microdroplets with quantitative phase imaging," *Langmuir* **31**(40), 11020 (2015).
- <sup>4</sup>L. Zhai, M. C. Berg, F. C. Cebeci, Y. Kim, J. M. Milwid, M. F. Rubner, and R. E. Cohen, "Patterned superhydrophobic surfaces: Toward a synthetic mimic of the Namib Desert beetle," *Nano Lett.* **6**(6), 1213 (2006).
- <sup>5</sup>Q. Li, Y. T. Zhu, I. A. Kinloch, and A. H. J. Windle, "Self-organization of carbon nanotubes in evaporating droplets," *J. Phys. Chem. B* **110**(28), 13926 (2006).
- <sup>6</sup>J. Kim, J. A. Hanna, M. Byun, C. D. Santangelo, and R. C. Hayward, "Designing responsive buckled surfaces by halftone gel lithography," *Science* **335**(6073), 1201 (2012).
- <sup>7</sup>M. A. Burns, "An integrated nanoliter DNA analysis device," *Science* **282**, 484 (1998).

- <sup>8</sup>V. Dugas, J. Broutin, and E. Souteyrand, "Droplet evaporation study applied to DNA chip manufacturing," *Langmuir* **21**(20), 9130 (2005).
- <sup>9</sup>N. J. Cira, A. Benusiglio, and M. Prakash, "Vapour-mediated sensing and motility in two-component droplets," *Nature* **519**, 446 (2015).
- <sup>10</sup>A. Shaikkea, S. Basu, S. Hatte, and L. Bansal, "Insights into vapor-mediated interactions in a nanocolloidal droplet system: evaporation dynamics and effects on self-assembly topologies on macro-to micro-scales," *Langmuir* **32**(40), 10334 (2016).
- <sup>11</sup>T. K. Pradhan and P. K. Panigrahi, "Deposition pattern of interacting droplets," *Colloids Surf. A: Physicochem. Eng. Aspects* **482**, 562 (2015).
- <sup>12</sup>R. D. Deegan, O. Bakajin, T. F. Dupont, G. Huber, S. R. Nagel, and T. A. Witten, "Contact line deposits in an evaporating drop," *Phys. Rev. E* **62**, 756 (2000).
- <sup>13</sup>L. Chen and J. R. Evans, "Arched structures created by colloidal droplets as they dry," *Langmuir* **25**(19), 11299 (2009).
- <sup>14</sup>J. Pierre, C. Cottin-Bizonne, J.-M. Benoit, C. Ybert, C. Journet, P. Tabeling, and L. Bocquet, "Slippage of water past superhydrophobic carbon nanotube forests in microchannels," *Phys. Rev. Lett.* **97**(15), 156104 (2006).
- <sup>15</sup>O. Ozen, N. Aubry, D. T. Papageorgiou, and P. G. Petropoulos, "Monodisperse drop formation in square microchannels," *Phys. Rev. Lett.* **96**(14), 144501 (2006).
- <sup>16</sup>T. Ous and C. Arcoumanis, "The formation of water droplets in an air-breathing PEMFC," *Int. J. Hydrogen Energy* **34**(8), 3476 (2009).
- <sup>17</sup>L. Bansal, S. Chakraborty, and S. Basu, "Confinement-induced alterations in the evaporation dynamics of sessile droplets," *Soft Matter* **13**(5), 969 (2017).
- <sup>18</sup>R. G. Picknett and R. Bexon, "The evaporation of sessile or pendant drops in still air," *J. Colloid Interface Sci.* **61**(2), 336 (1977).
- <sup>19</sup>H. Y. Erbil, "Evaporation of pure liquid sessile and spherical suspended drops: A review," *Adv. Colloid Interface Sci.* **170**(1), 67 (2012).
- <sup>20</sup>D. Hu and H. Wu, "Volume evolution of small sessile droplets evaporating in stick-slip mode," *Phys. Rev. E* **93**(4), 042805 (2016).
- <sup>21</sup>A. J. D. Shaikkea and S. Basu, "Insight into the evaporation dynamics of a pair of sessile droplets on a hydrophobic substrate," *Langmuir* **32**(5), 1309 (2016).
- <sup>22</sup>S. Dash and S. V. Garimella, "Droplet evaporation dynamics on a superhydrophobic surface with negligible hysteresis," *Langmuir* **29**(34), 10785 (2013).